

MicroRNAs 103 and 107 regulate insulin sensitivity

TRAJKOVSKI, Mirko, *et al.*

Abstract

Defects in insulin signalling are among the most common and earliest defects that predispose an individual to the development of type 2 diabetes. MicroRNAs have been identified as a new class of regulatory molecules that influence many biological functions, including metabolism. However, the direct regulation of insulin sensitivity by microRNAs in vivo has not been demonstrated. Here we show that the expression of microRNAs 103 and 107 (miR-103/107) is upregulated in obese mice. Silencing of miR-103/107 leads to improved glucose homeostasis and insulin sensitivity. In contrast, gain of miR-103/107 function in either liver or fat is sufficient to induce impaired glucose homeostasis. We identify caveolin-1, a critical regulator of the insulin receptor, as a direct target gene of miR-103/107. We demonstrate that caveolin-1 is upregulated upon miR-103/107 inactivation in adipocytes and that this is concomitant with stabilization of the insulin receptor, enhanced insulin signalling, decreased adipocyte size and enhanced insulin-stimulated glucose uptake. These findings demonstrate the central importance of miR-103/107 to [...]

Reference

TRAJKOVSKI, Mirko, *et al.* MicroRNAs 103 and 107 regulate insulin sensitivity. *Nature*, 2011, vol. 474, no. 7353, p. 649-53


PMID : 21654750

DOI : 10.1038/nature10112

Available at:

<http://archive-ouverte.unige.ch/unige:30806>

Disclaimer: layout of this document may differ from the published version.



MicroRNAs 103 and 107 regulate insulin sensitivity

Mirko Trajkovski^{1,2}, Jean Hausser^{2,3}, Jürgen Soutschek⁴, Bal Bhat⁴, Akinc Akin⁵, Mihaela Zavolan³, Markus H. Heim^{2,6} & Markus Stoffel^{1,2}

Defects in insulin signalling are among the most common and earliest defects that predispose an individual to the development of type 2 diabetes^{1–3}. MicroRNAs have been identified as a new class of regulatory molecules that influence many biological functions, including metabolism^{4,5}. However, the direct regulation of insulin sensitivity by microRNAs *in vivo* has not been demonstrated. Here we show that the expression of microRNAs 103 and 107 (miR-103/107) is upregulated in obese mice. Silencing of miR-103/107 leads to improved glucose homeostasis and insulin sensitivity. In contrast, gain of miR-103/107 function in either liver or fat is sufficient to induce impaired glucose homeostasis. We identify caveolin-1, a critical regulator of the insulin receptor, as a direct target gene of miR-103/107. We demonstrate that caveolin-1 is upregulated upon miR-103/107 inactivation in adipocytes and that this is concomitant with stabilization of the insulin receptor, enhanced insulin signalling, decreased adipocyte size and enhanced insulin-stimulated glucose uptake. These findings demonstrate the central importance of miR-103/107 to insulin sensitivity and identify a new target for the treatment of type 2 diabetes and obesity.

To identify microRNAs (miRNAs) that are deregulated in obesity and insulin resistance, we performed miRNA microarray analysis on the livers of two types of obese mice: *ob/ob* mice and diet-induced-obese (DIO) C57BL/6J mice (Supplementary Table 1a–c). The miR-103/miR-107 family was among the five most-upregulated miRNAs in the livers of both obese models, and the expression of these miRNAs was also reportedly increased in diabetic Goto-Kakizaki rats⁶. The expression levels were validated by northern blotting, demonstrating a twofold to threefold upregulation in the livers of both models (Fig. 1a). The sequences of mature miR-103 and miR-107 differ by one nucleotide at position 21 and cannot be discriminated by northern blotting. By real-time PCR, we could distinguish miR-103 and miR-107 and show that both miRNAs are upregulated in the livers of *ob/ob* and DIO mice (Supplementary Fig. 1a–d). We also measured the expression of these miRNAs in liver biopsies from a cohort of human patients. miR-103 and miR-107 levels were similar in normal subjects and in subjects with viral hepatitis, but increased in alcoholic liver disease (ALD), non-alcoholic fatty liver disease (NAFLD) and non-alcoholic steatohepatitis (NASH), conditions often associated with diabetes⁷. Furthermore, there was a positive correlation between the subjects' homeostatic model assessment (HOMA) index and miR103/107 expression levels (Fig. 1b and Supplementary Fig. 2a–c), indicating an association of these miRNAs with insulin resistance.

To investigate the effect of elevated miR-103/107 expression, we generated recombinant adenovirus expressing miR-107 (ad-107/GFP). Injection of wild-type mice with ad-107/GFP (Supplementary Fig. 3a, b) caused a rise in both random and fasting blood-glucose levels, and also in insulin levels (Fig. 1c, d). It impaired glucose tolerance after an intra-peritoneal glucose injection and decreased insulin sensitivity relative to that in control ad-GFP-infected mice (Fig. 1e, f). Hepatic overexpression of miR-107 resulted in increased glucose production during an intraperitoneal pyruvate-tolerance test

(Fig. 1g). The increase in hepatic glucose production was accompanied by augmented expression of glucose 6-phosphatase, phosphoenolpyruvate carboxykinase, pyruvate carboxylase and fructose 1,6-biphosphatase, indicating that increased gluconeogenesis is the primary cause of the elevated glucose levels (Fig. 1h). These data show that gain-of-function of miR-107 in the liver decreases insulin sensitivity and enhances hepatic glucose production.

To study the effect of miR-103/107 silencing, we first tested whether antagomirs⁸ would inhibit both miR-103 and miR-107. Northern blot analysis of miR-103 and miR-107 showed that antagomir-103 (ant-103) effectively and specifically silenced both miRNAs in liver and fat (Supplementary Fig. 3c, d). Markers for liver damage and inflammation were unaffected by the treatment (data not shown). Application of ant-103 did not affect blood glucose levels in chow-fed wild-type mice but it did lower plasma glucose levels in *ob/ob* mice when compared to mice treated with PBS or with the controls ant-124 (scrambled) or mismatch-ant-103 (ant-MM103) (Fig. 2a, b). Similar effects were observed in DIO mice (Fig. 2c). Glucose-tolerance and insulin-tolerance tests showed that there was improved glucose tolerance and insulin sensitivity in both *ob/ob* and DIO mice that were injected with ant-103 (Fig. 2d–f). A pyruvate-tolerance test revealed that *de novo* hepatic glucose production was reduced (Fig. 2g) and this finding was supported by a reduction in hepatic expression of glucose 6-phosphatase, pyruvate carboxylase and fructose 1,6-biphosphatase in ant-103-treated mice (Fig. 2h). In addition, liver glycogen content was increased and plasma insulin levels were decreased in ant-103-treated *ob/ob* and DIO animals (Fig. 2i, j). Metabolic and energy-expenditure studies carried out in metabolic cages showed that *ob/ob* mice lacking miR-103 expression had increased O₂ consumption and CO₂ production, as well as moderately elevated body temperature, but that their food intake was similar to control mice. Gene expression analysis in adipocytes from ant-103-treated mice revealed increased levels of β -oxidation genes (carnitine palmitoyltransferase 1a (*Cpt1a*), peroxisomal acyl-coenzyme A oxidase 3 (*Acox3*) and very long chain acyl-coenzyme A dehydrogenase (*Acadvl*)) but there were no changes in the lipogenic genes acetyl-coenzyme A carboxylase alpha and beta (*Acaca* and *Acacb*, also known as *Acc1* and *Acc2*) (Supplementary Fig. 4a–d). Two independent indicators of insulin sensitivity, the glucose infusion rate and clamp glucose turnover, were improved during hyperinsulinaemic-euglycaemic clamp studies in ant-103-treated *ob/ob* mice compared to PBS-injected controls. Hepatic glucose production was decreased and glucose uptake in adipose tissue was enhanced in ant-103-treated animals. In contrast, treatment with ant-103 did not improve glucose uptake in skeletal muscle (Supplementary Table 2). Together, these data demonstrate that silencing of miR-103/107 enhances insulin sensitivity in liver and adipose tissue.

To test the contribution of the liver to the effect on insulin sensitivity, we delivered ant-103 and control ant-MM103 specifically to the liver through liposomal formulations. Liposomal ant-103 induced the specific silencing of miR-103 in the liver, but not in fat and muscle. Silencing of miR-103/107 in the livers of *ob/ob* mice had no effect on

¹Institute for Molecular Systems Biology, ETH Zurich, Wolfgang-Pauli Strasse 16, CH-8093 Zurich, Switzerland. ²Competence Center of Systems Physiology and Metabolic Disease, ETH Zurich, Schafmattstrasse 18, HPM F 39.1 CH-8093 Zurich, Switzerland. ³Biozentrum Basel, University of Basel, Klingelbergstrasse 50/70, CH-4056 Basel, Switzerland. ⁴Regulus Therapeutics Inc., 3545 John Hopkins Court, San Diego, California 92121-1121, USA. ⁵Alnylam Pharmaceuticals, 300 Third Street, Cambridge, Massachusetts 02142, USA. ⁶University Hospital Basel, Hebelstrasse 20, CH-4031 Basel, Switzerland.

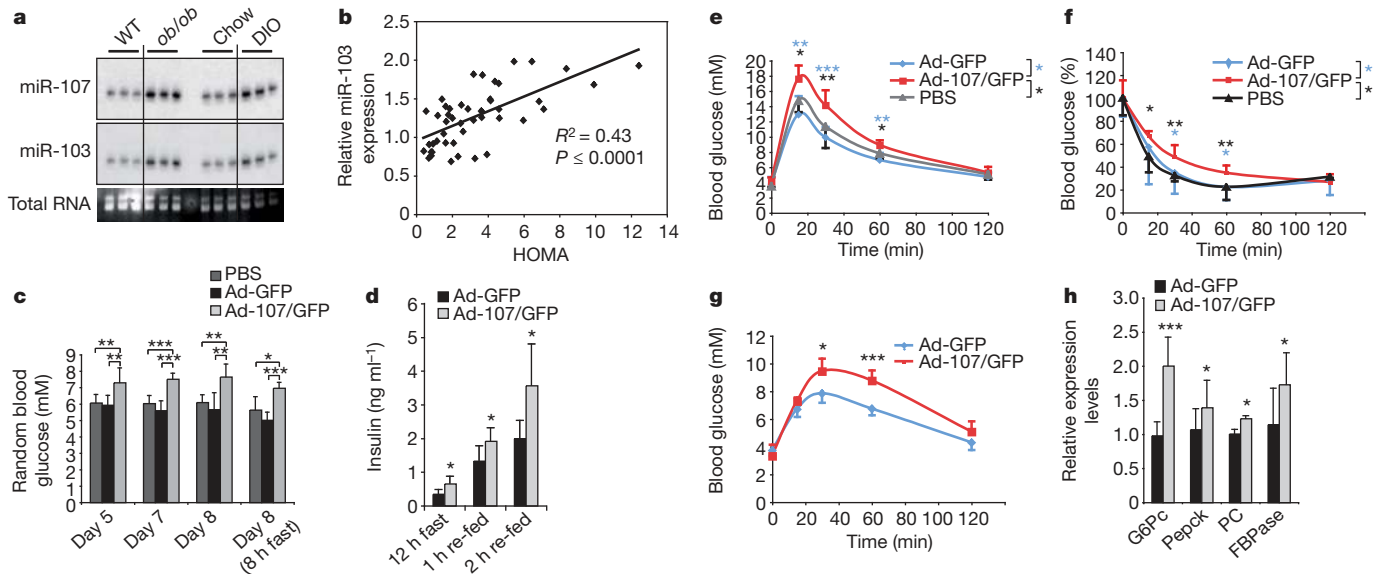


Figure 1 | Hepatic overexpression of miR-107 induces hyperglycaemia. **a**, Northern blot of liver RNA from C57BL/6J (WT), *ob/ob*, chow-fed or DIO mice, as indicated ($n = 3$). The loading control labelled 'total RNA' is stained with ethidium bromide. **b**, Correlation between relative miR-103 levels (Rel. miR-103) and HOMA index in a group of humans including healthy individuals ($n = 6$), chronic hepatitis B and hepatitis C virus-infected individuals (HBV, $n = 6$; HCV, $n = 7$), patients with alcoholic steatohepatitis ($n = 4$), patients with non-alcoholic fatty liver disease ($n = 13$) and patients with non-alcoholic steatohepatitis ($n = 13$). **c**, Blood glucose levels of C57BL/6J mice injected with

PBS, ad-GFP or ad-107/GFPBL/ ($n = 6$). **d**, Plasma insulin levels of C57BL/6J mice treated as in **c**, after a 12 h fast followed by re-feeding. **e–g**, Glucose-tolerance test (**e**), insulin-tolerance test (**f**) and pyruvate-tolerance test (**g**) in mice injected with ad-GFP or ad-107/GFP. **h**, Relative mRNA expression of genes encoding glucose 6-phosphatase (G6Pc), phosphoenol-pyruvate carboxykinase (Pepck), pyruvate carboxylase (PC) and fructose 1,6-bisphosphatase (FBPase) from livers of mice as in **e–g**. Expression is normalized to the *36B4* gene, encoding the acidic ribosomal phosphoprotein P0 (RPLP0) ($n = 5$). Means \pm s.d. are shown for all panels. *, $P < 0.05$; **, $P < 0.01$; ***, $P < 0.001$.

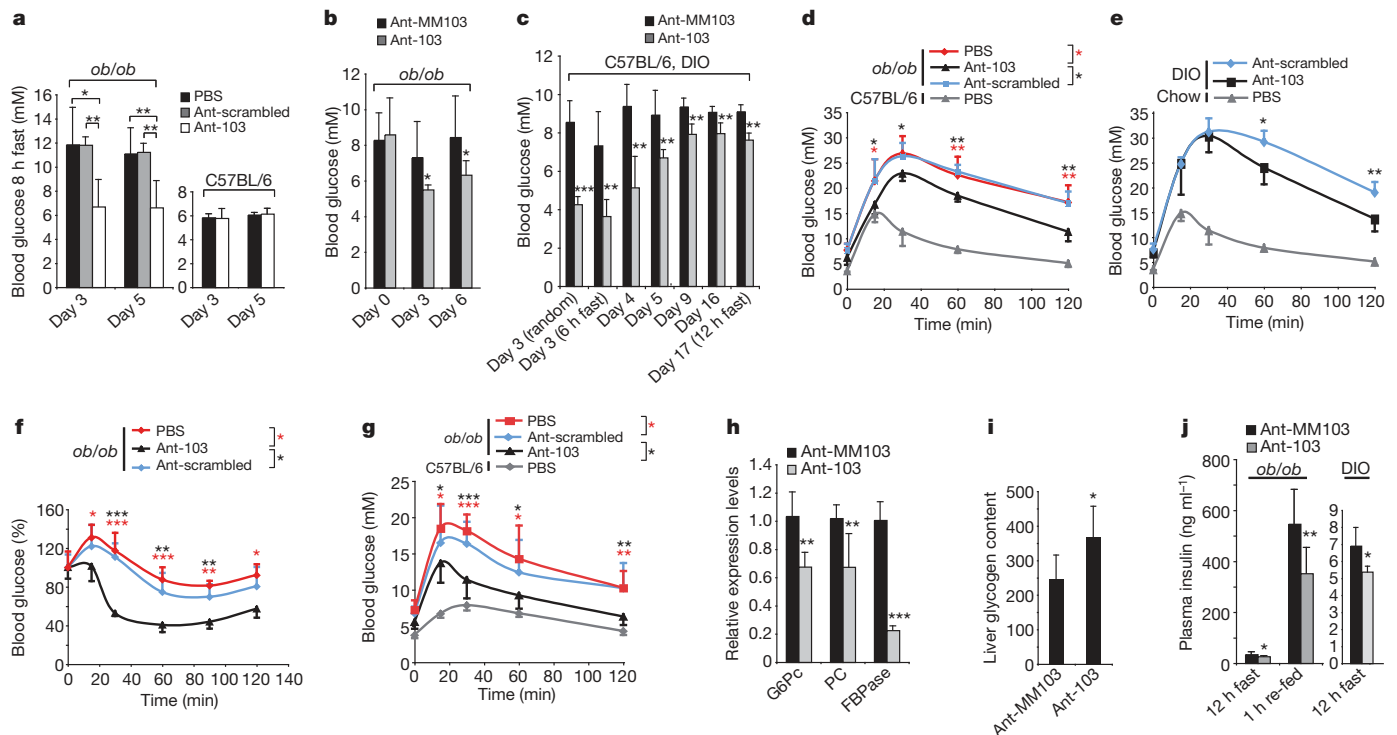


Figure 2 | Silencing of miR-103 and miR-107 alleviates hyperglycaemia in diabetic mice. **a–c**, Blood glucose levels of ant-103-treated or control-treated (PBS, scrambled or ant-MM103) *ob/ob* ($n = 6$), C57BL/6J ($n = 5$) or DIO ($n = 5$) mice. Days after treatment and random or fasting conditions are noted for each measurement. **d, e**, Glucose-tolerance tests in control or ant-103-injected *ob/ob* (**d**) or DIO (**e**) mice compared to control C57BL/6J or chow-fed mice ($n = 5$). **f, g**, Insulin-tolerance test (**f**) or pyruvate-tolerance test (**g**) in control or ant-103-injected *ob/ob* mice ($n = 5$). In **f**, values at the zero time

point are normalized to 100%. **h**, Relative mRNA expression of the genes for G6Pc, PC and FBPase in livers of *ob/ob* mice 16 d after injection with ant-MM103 or ant-103 ($n = 5$). **i**, Liver glycogen content in *ob/ob* mice 16 d after injection with ant-MM103 or ant-103 ($n = 5$). **j**, Insulin levels in *ob/ob* mice (left, $n = 10$) or DIO mice (right, $n = 5$) 10 d after injection of ant-MM103 or ant-103. In **d, e** and **g**, PBS-injected C57BL/6J mice ($n = 5$) are shown as controls. Means \pm s.d. are shown for all panels. *, $P < 0.05$; **, $P < 0.01$; ***, $P < 0.001$.

blood glucose levels, plasma insulin levels or glucose-tolerance, insulin-tolerance and pyruvate-tolerance tests (Supplementary Fig. 5a–f), indicating that silencing of miR-103/107 in the liver is not sufficient to reverse insulin resistance in obese mice. Because the expression of miR-103 is about eightfold higher in adipose tissue than in liver and muscle, we examined the effect of miR-103/107 silencing in adipose tissue. Obese (*ob/ob*) mice showed a slight reduction in body weight when miR-103/107 were systemically silenced (Supplementary Fig. 6a). In contrast, specific manipulation of hepatic miR-103/107 expression using liposomal ant-103 or Ad-107/GFP did not affect body weight when compared to that of control-treated mice (data not shown). We therefore used computer tomography to investigate the fat distribution of DIO and *ob/ob* animals after miR-103 silencing. Both DIO and *ob/ob* mice treated with ant-103 showed reduced levels of total fat, owing to a decrease in both subcutaneous and visceral adipose tissue (Fig. 3a, b). Furthermore, organ measurements revealed a decrease in inguinal fat-pad weights in the ant-103-treated group but no weight differences in other organs (Supplementary Fig. 6b). To investigate whether this reduction was due to lower cell numbers or smaller adipocytes, we quantified the mean size of adipocytes from fat tissue sections using automated image-analysis software. Ant-103-treated DIO and *ob/ob* animals had smaller adipocytes than ant-MM103-injected controls (Fig. 3c, d), owing to an increased number of small adipocytes and a decreased number of large ones (Supplementary Fig. 6c–f). A comparison between the decrease in fat-pad size, measured by computer tomography, and the average decrease in adipocyte size showed that ant-103-treated mice had approximately 10–20% more adipocytes than ant-MM103-treated controls.

Because miR-103 has been implicated in adipocyte differentiation^{9–13}, we explored whether the increase in adipocyte number in miR-103-depleted mice could be attributed to changes in pre-adipocyte differentiation. We induced adipocyte differentiation of isolated stromal-vascular cells from both visceral and subcutaneous fat in the presence of either ant-103 or ant-MM103. Quantification of mature adipocyte numbers by high-content imaging after 8 d in culture demonstrated a 2-fold and 2.5-fold increase in the number of differentiated adipocytes in the ant-103-treated stromal-vascular cells derived from visceral and subcutaneous fat, respectively. This indicates that the absence of miR-103 enhances adipocyte differentiation in a cell-autonomous fashion. Conversely, overexpression of miR-107 decreased the number of differentiated adipocytes (Fig. 3e). The negative effect of miR-103 on pre-adipocyte differentiation was further corroborated by gene expression analysis of an early marker of adipocyte differentiation, CCAAT/enhancer binding protein (C/EBP)- β (*Cebpb*), and of two late markers of adipocyte differentiation, peroxisome proliferator activated receptor- γ (*Pparg*) and adipocyte fatty acid binding protein 4 (*Fabp4*) (Fig. 3f–h).

To test whether fat-specific overexpression of miR-107 affects insulin sensitivity, we injected either ad-107/GFP or ad-GFP into the inguinal fat pads of wild-type mice. The relative size of the inguinal fat deposit was $20.7 \pm 6.3\%$ of total body fat, as determined by computer tomography. Expression of miR-107 was increased by about 1.6-fold and was restricted to the fat pad. Levels of blood glucose and insulin in mice injected with ad-107/GFP were increased and glucose-tolerance and insulin-tolerance tests showed decreased glucose tolerance and insulin sensitivity, respectively, supported by an increase in the HOMA index. Furthermore, adipocyte size was increased in the fat pads injected with ad-miR-107, compared to the ad-GFP controls (Supplementary Fig. 7a–g). These data show that overexpression of miR-107 in the fat is sufficient to induce insulin resistance and glucose intolerance.

Smaller adipocytes are associated with increased insulin sensitivity in human and rodent models¹⁴. To explore whether insulin-stimulated glucose uptake in adipocytes was affected by miR-103 silencing, we isolated primary adipocytes from *ob/ob* mice injected with either ant-103 or ant-MM103 and measured insulin-stimulated D-¹⁴C-glucose

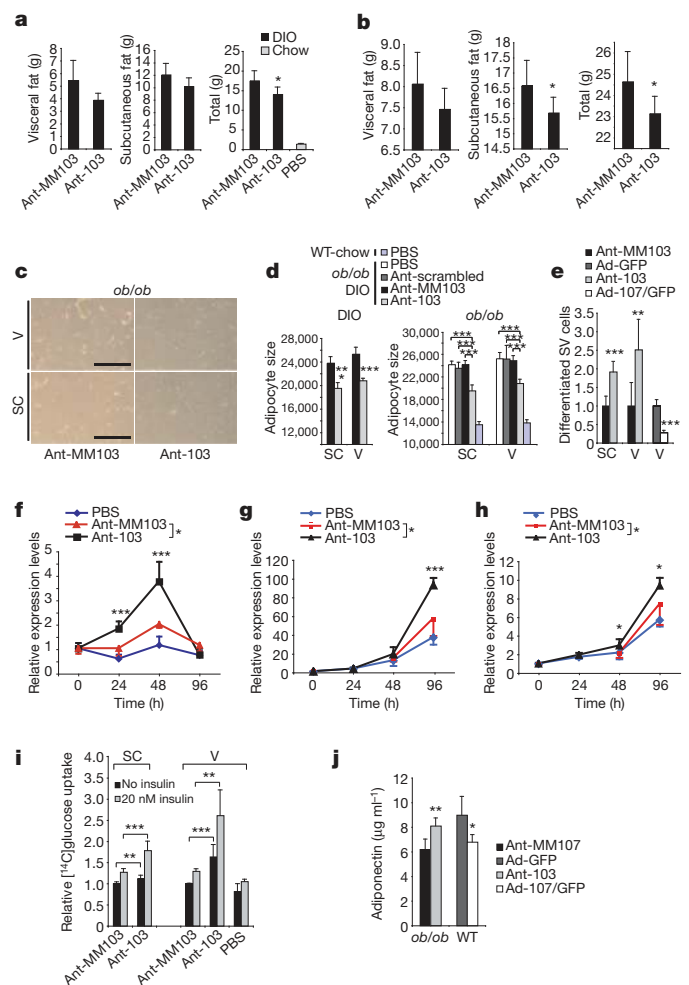


Figure 3 | Silencing of miR-103 decreases total fat by reducing adipocyte size. **a, b**, Fat-pad weights from subcutaneous and visceral adipose tissue of mice injected with ant-MM103 or ant-103. DIO mice (**a**, $n = 4 + 5$, respectively) or *ob/ob* mice (**b**, $n = 6$) were assessed by computer tomography 13 d after injection. **c**, Haematoxylin staining of paraffin sections from subcutaneous (SC) and visceral (V) fat of *ob/ob* mice injected with ant-MM103 or ant-103. Scale bar: 250 μ m. **d**, Automated quantification of the average adipocyte size from mice treated as in **c**, with PBS and with ant-scrambled controls. **e**, Automated quantification of differentiated adipocytes after 8 days of differentiation in the presence of ant-103, ant-MM103, ad-GFP or ad-107/GFP. The values shown are normalized to 1. **f–h**, Relative mRNA levels (Rel. expression) of *Cebpb* (**f**), *Fabp4* (**g**) or *Pparg* (**h**) in stromal-vascular cells differentiated in the presence of PBS, ant-MM103 or ant-103, at the indicated time points. The mRNA expression levels at time point 0 were determined before the antagomir/differentiation treatment. **i**, [¹⁴C]Glucose uptake in primary adipocytes isolated from subcutaneous or visceral fat of *ob/ob* mice injected with PBS, ant-MM103 or ant-103. Uptake is normalized to cell numbers. **j**, Adiponectin levels in ant-MM103-injected or ant-103-injected *ob/ob* mice (left, $n = 7$), and in ad-GFP-injected or ad-107/GFP-injected C57BL/6J mice (right, $n = 9$). Means \pm s.d. are shown for all panels. *, $P < 0.05$; **, $P < 0.01$; ***, $P < 0.001$.

uptake *in vitro*. Basal and insulin-stimulated glucose uptake was increased in adipocytes from both subcutaneous and visceral fat of ant-103-injected animals (Fig. 3i). Furthermore, adiponectin levels, which correlate positively with insulin sensitivity¹⁵, were increased in ant-103-injected *ob/ob* mice (Fig. 3j). Together, these data show that silencing of miR-103/107 increases insulin sensitivity in adipocytes.

To address the possible mechanism by which miR-103 and miR-107 regulate insulin sensitivity, we performed genome-wide expression analysis using Affymetrix microarrays, comparing livers from C57BL/6J mice infected with ad-107/GFP or ad-GFP. In animals

infected with ad-107/GFP, mRNAs carrying a seed match to miR-107 in the 3' untranslated region (3' UTR) were downregulated when compared to transcripts that lacked a miR-107 seed. The data were confirmed by real-time PCR for a subset of miR-107 target genes (Fig. 4a). Out of over 3,000 genes with a 6-mer seed match in the 3' UTR, the predicted top 100 targets of miR-107/103 were enriched in membrane-related genes and metabolism genes (Supplementary Fig. 8a, b). The gene encoding caveolin-1 (*Cav1*), a key component of caveolae and a mediator of insulin signalling, was among the miR-103/107 seed-containing genes that were downregulated after overexpression of miR-107 in the liver, and upregulated after its silencing (Fig. 4a and Supplementary Fig. 8c). Notably, miR-103 silencing in the fat resulted in an approximately 3.5-fold upregulation of *Cav1* mRNA levels (Fig. 4b). Murine *Cav1* (*mCav1*) contains three miR-103 sites, whereas human *CAV1* (*hCAV1*) has two seed motifs in the 3' UTR (Supplementary Fig. 8d, e). Measurements of luciferase activity in HEK 293 cells transfected with reporter plasmids containing the 3' UTRs of *mCav1* or *hCAV1* showed reduced expression of these constructs in the presence of miR-103 (Fig. 4c). By mutating the conserved seed, we could fully reverse the miR-103-induced decrease in luciferase activity in both *mCav1* and *hCAV1* constructs (Fig. 4c). Overexpression of miR-103 also led to an approximately twofold decrease in endogenous *Cav1* levels in HEK 293 cells compared to controls (Fig. 4d). Conversely, ant-103, but not ant-scrambled or PBS controls, increased *Cav1* levels in HEK 293 cells (Fig. 4e).

Taken together, these data demonstrate that *Cav1* is a direct target of miR-103 in both mouse and human cells.

Cav1 is the principal protein of caveolae¹⁶, distinct lipid- and cholesterol-enriched vascular invaginations at the plasma membrane. *Cav1* activates insulin signalling, probably by stabilizing caveolae and their associated insulin receptors¹⁷. Peptides corresponding to the scaffolding domain of *Cav1* and *Cav3* potently stimulate insulin-receptor-kinase activity¹⁸. Furthermore, overexpression of *Cav3* augments insulin-stimulated phosphorylation of insulin receptor substrate 1 (ref. 18) and increases hepatic insulin-receptor phosphorylation in response to insulin stimulation, thereby improving the overall glucose metabolism of diabetic mice¹⁹. *Cav1*-null mice are phenotypically normal on a chow diet but develop insulin resistance on a high-fat diet owing to decreased insulin-receptor expression and diminished insulin-receptor signalling in adipose tissue²⁰. We investigated whether insulin signalling correlated with miR-103/107-mediated changes in *Cav1* expression. In the fat and liver of *ob/ob* mice, silencing of miR-103/107 resulted in increased *Cav1* levels, whereas no expression of this protein could be detected in skeletal muscle (Fig. 4f–h). The expression of insulin receptor β -subunit (IR β) in adipocytes was increased and insulin-stimulated levels of phosphorylated Akt1 and IR β (pAkt1 and pIR β) were augmented in the fat and liver of ant-103-treated mice (Fig. 4f, g). In contrast, insulin signalling was not enhanced in the skeletal muscle of ant-103-treated mice (Fig. 4h). In addition, wild-type mice in which ad-miR-107 was injected into the inguinal fat pad

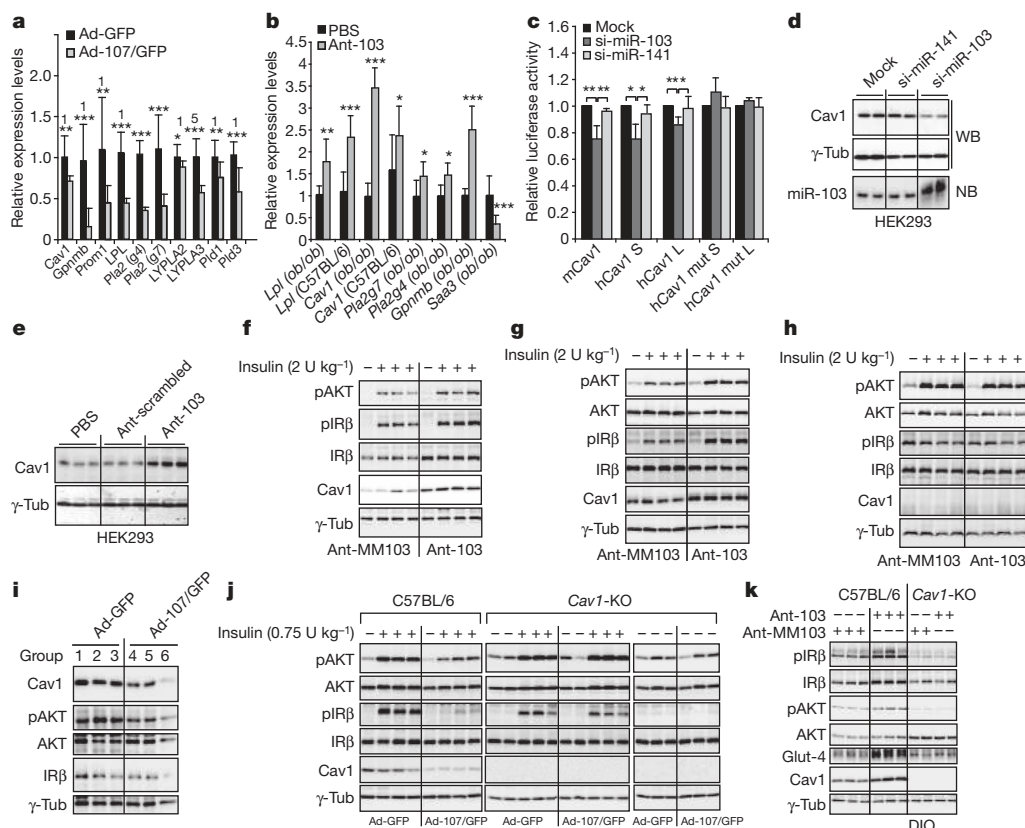


Figure 4 | Regulation of gene expression and insulin signalling by miR-103. **a, b**, Gene expression analysis (relative expression) in livers from C57BL/6J mice 10 d after injection with ad-GFP or ad-107/GFP (**a**, $n = 5$), or in fat from *ob/ob* mice injected with PBS or ant-103 (**b**, $n = 5$). **c**, Relative luciferase activity in HEK 293 cells transfected with reporter constructs containing the 3' UTR of *Cav1*, co-transfected with si-miR-103, si-miR-141 (scrambled) or PBS (Mock). S, short; L, long; mut, mutant. **d**, Western blotting (WB) and northern blotting (NB) of HEK 293 cells transfected with PBS, si-miR-141 (scrambled) or si-miR-103. γ -Tub, γ -Tubulin. **e**, Immunoblotting of protein extracts from HEK 293 cells transfected with PBS, control ant-scrambled or ant-103. **f–h**, Immunoblotting of protein extracts from fat (**f**), liver (**g**) or muscle (**h**) of

ant-MM103-injected or ant-103-injected *ob/ob* mice stimulated with 2 U kg⁻¹ insulin for 8 min. **i**, Western blot analysis of perigon fat pads in C57BL/6J mice surgically injected with ad-GFP or ad-107/GFP. Each lane represents a pool of two mice. **j**, Western blot analysis of liver extracts from C57BL/6J or *Cav1*-knockout (*Cav1*-KO) mice injected with ad-GFP or ad-107/GFP, stimulated with 0.75 U kg⁻¹ insulin for 10 min after a 12 h fast. **k**, Immunoblotting of protein extracts from the fat of DIO C57BL/6J or DIO *Cav1*-KO mice 8 d after injection with ant-MM103 or ant-103 and stimulated for 8 min with 1.2 U kg⁻¹ insulin after a 12 h fast. Animals were kept on a high-fat diet for 5 weeks before antagomir injection. Glut-4, glucose transporter-4. Means \pm s.d. are shown for all panels. *, $P < 0.05$; **, $P < 0.01$; ***, $P < 0.001$.

showed a reduction in Cav1 expression and decreased IR β and pAkt1 levels (Fig. 4i). We also studied insulin signalling in the livers of mice with miR-107 overexpression. Cav1 and pAkt1 levels were diminished in the livers of wild-type mice infected with ad-miR-107, with no changes observed in IR β protein levels (Fig. 4j). This result is in agreement with our findings showing that overexpression of miR-107 can induce hepatic insulin resistance, and with data from Cav1-null mice, which maintain normal IR β levels in the liver but show reduced IR β and pAkt1 levels in fat^{19–21}.

Finally, to investigate whether modulation of Cav1 expression by miR-107 is important for the observed phenotypes, we overexpressed or silenced miR-103/107 in DIO Cav1-null mice. Whereas hepatic overexpression of miR-107 in wild-type mice led to impaired glucose tolerance, no significant effects on plasma glucose, glucose-tolerance, insulin-tolerance or pyruvate-tolerance tests were measured when Cav1-null mice were injected with ad-107/GFP and compared to ad-GFP-treated Cav1-null animals (Supplementary Fig. 9a–d). Furthermore, no molecular changes in insulin signalling events were detected in the two groups (Fig. 4j). Administration of ant-103 to DIO Cav1-null mice also did not affect glucose tolerance, insulin sensitivity or phosphorylation of insulin receptor and Akt1 upon insulin stimulation (Fig. 4k and Supplementary Fig. 9e–h). However, expression of lipolytic genes in the adipose tissue of Cav1-null mice was still responsive to treatment with ant-103, compared to ant-MM103 (Supplementary Fig. 9i), indicating that miR-103/107 also mediate some Cav1-independent metabolic effects.

Our findings show that miR-103 and miR-107 are negative regulators of insulin sensitivity. Their increased hepatic expression in rodents and humans with insulin resistance and hepatic steatosis indicates that they might contribute to the aetiology of diabetes. We also show that global miR-103/107 silencing causes increased insulin signalling in both liver and adipose tissue, although silencing of hepatic miR-103/107 expression in overt obese and insulin-resistant states is insufficient to reverse the metabolic abnormalities. This indicates that silencing of miR-103 in adipocytes is the dominant contributor to enhanced insulin sensitivity. One mechanism by which these miRNAs regulate insulin sensitivity is by targeting Cav1, thereby diminishing the number of insulin receptors in caveolae-enriched plasma membrane microdomains and reducing downstream insulin signaling. It is likely that Cav1 also mediates other effects that contribute to the phenotype because this protein has many functions in growth-factor signalling, endocytotic pathways and lipid regulation²². Our finding that silencing miR-103/107 in obese animals improves glucose homeostasis implicates these miRNAs as novel therapeutic targets for the treatment of diabetes.

METHODS SUMMARY

Animals. All mice were males and were maintained on a C57BL/6J background, on a 12-h light/dark cycle in a pathogen-free animal facility. Antagomirs at doses of 15 mg kg⁻¹ in 0.2 ml total volume with PBS per injection were administered on two consecutive days through the tail vein of wild-type or *ob/ob* mice at between 6 and 8 weeks of age, or to 12-week-old DIO mice fed on a diet containing 60% fat (Pvolimi Kliba AG) for 8 weeks. Mice were injected with adenoviruses through the tail vein at 1×10^9 plaque-forming units in 0.2 ml PBS. Injection of ad-107/GFP and antagomirs did not effect food consumption compared to that of control-treated animals. Mice were killed 10 d after the adenovirus injection. All animal studies were approved by the Kantonale Veterinärämte Zürich.

Antagomirs. The single-stranded RNAs and modified RNA analogues used in this study consisted of 21–23 nucleotides with modifications as specified: antagomir-103, 5'-u₃c₃uagcccuuacuuagcu₃g₃c₃u₃-Chol-3'; antagomir-107, 5'-u₃g₃uagcccuuacuuagcu₃g₃c₃u₃-Chol-3'; MM-antagomir-103, 5'-u₃g₃acagccuugacuuagcu₃g₃c₃u₃-Chol-3'; antagomir-124 (scrambled), 5'-g₃g₃cauucacccgucg₃u₃u₃a₃-Chol-3'. The lower-case letters represent 2'-O-Me-modified nucleotides; subscript 's' represents a phosphorothioate linkage; 'Chol' represents cholesterol linked through a hydroxypropylol linkage¹².

Lipid nanoparticle formulations. Liver-targeting lipid nanoparticle formulations of antagomirs were prepared using the novel ionizable lipid DLin-KC2-DMA (ref. 22). Lipid nanoparticles were composed of DLin-KC2-DMA, distearoyl phosphatidylcholine, cholesterol and mPEG2000-DMG, used at the molar ratio

50:10:38.5:1.5. Antagomirs were formulated in lipid nanoparticles at a total lipid-to-antagomir weight ratio of approximately 11:1.

Generation of recombinant adenovirus. Ad-107/GFP was generated by inserting the PCR-amplified miRNA precursor sequence generated with primers 5'-AATACCCGCATGGAAGCAGGCTAA-3' and 5'-AACATGTCTCAAGGAGAGGACGGT-3' into a GFP-expressing shuttle vector, Ad5CMV K-NpA. Ad-GFP (ViraQuest) was used as a control.

Statistical analysis. Unless otherwise specified, all bars show mean \pm s.d. Significance was calculated using student's *t*-test (*, *P* < 0.05; **, *P* < 0.01; ***, *P* < 0.001).

Full Methods and any associated references are available in the online version of the paper at www.nature.com/nature.

Received 22 March 2010; accepted 13 April 2011.

Published online 8 June 2011.

- Kahn, C. R. Knockout mice challenge our concepts of glucose homeostasis and the pathogenesis of diabetes. *Exp. Diabetes Res.* **4**, 169–182 (2003).
- Taniguchi, C. M., Emanuelli, B. & Kahn, C. R. Critical nodes in signalling pathways: insights into insulin action. *Nature Rev. Mol. Cell Biol.* **7**, 85–96 (2006).
- Muoio, D. M. & Newgard, C. B. Mechanisms of disease: molecular and metabolic mechanisms of insulin resistance and β -cell failure in type 2 diabetes. *Nature Rev. Mol. Cell Biol.* **9**, 193–205 (2008).
- Bartel, D. P. MicroRNAs: target recognition and regulatory functions. *Cell* **136**, 215–233 (2009).
- Krützfeldt, J. & Stoffel, M. MicroRNAs: a new class of regulatory genes affecting metabolism. *Cell Metab.* **4**, 9–12 (2006).
- Herrera, B. M. *et al.* Global microRNA expression profiles in insulin target tissues in a spontaneous rat model of type 2 diabetes. *Diabetologia* **53**, 1099–1109 (2010).
- Anderson, N. & Borlak, J. Molecular mechanisms and therapeutic targets in steatosis and steatohepatitis. *Pharmacol. Rev.* **60**, 311–357 (2008).
- Krützfeldt, J. *et al.* Silencing of microRNAs *in vivo* with 'antagomirs'. *Nature* **438**, 685–689 (2005).
- Esau, C. *et al.* MicroRNA-143 regulates adipocyte differentiation. *J. Biol. Chem.* **279**, 52361–52365 (2004).
- Kajimoto, K., Naraba, H. & Iwai, N. MicroRNA and 3T3-L1 pre-adipocyte differentiation. *RNA* **12**, 1626–1632 (2006).
- Ortega, F. J. *et al.* MiRNA expression profile of human subcutaneous adipose and during adipocyte differentiation. *PLoS ONE* **5**, e9022 (2010).
- Sun, T., Fu, M., Bookout, A. L., Klier, S. A. & Mangelsdorf, D. J. MicroRNA let-7 regulates 3T3-L1 adipogenesis. *Mol. Endocrinol.* **23**, 925–931 (2009).
- Xie, H., Lim, B. & Lodish, H. F. MicroRNAs induced during adipogenesis that accelerate fat cell development are downregulated in obesity. *Diabetes* **58**, 1050–1057 (2009).
- Goossens, G. H. The role of adipose tissue dysfunction in the pathogenesis of obesity-related insulin resistance. *Physiol. Behav.* **94**, 206–218 (2008).
- Yamauchi, T. *et al.* The fat-derived hormone adiponectin reverses insulin resistance associated with both lipodystrophy and obesity. *Nature Med.* **7**, 941–946 (2001).
- Rothberg, K. G. *et al.* Caveolin, a protein component of caveolae membrane coats. *Cell* **68**, 673–682 (1992).
- Nystrom, F. H., Chen, H., Cong, L. N., Li, Y. & Quon, M. J. Caveolin-1 interacts with the insulin receptor and can differentially modulate insulin signaling in transfected Cos-7 cells and rat adipose cells. *Mol. Endocrinol.* **13**, 2013–2024 (1999).
- Yamamoto, M. *et al.* Caveolin is an activator of insulin receptor signaling. *J. Biol. Chem.* **273**, 26962–26968 (1998).
- Otsu, K. *et al.* Caveolin gene transfer improves glucose metabolism in diabetic mice. *Am. J. Physiol. Cell Physiol.* **298**, C450–C456 (2009).
- Cohen, A. W. *et al.* Caveolin-1-deficient mice show insulin resistance and defective insulin receptor protein expression in adipose tissue. *Am. J. Physiol. Cell Physiol.* **285**, C222–C235 (2003).
- Cohen, A. W., Combs, T. P., Scherer, P. E. & Lisanti, M. P. Role of caveolin and caveolae in insulin signaling and diabetes. *Am. J. Physiol. Endocrinol. Metab.* **285**, E1151–E1160 (2003).
- Parton, R. G. & Simons, K. The multiple faces of caveolae. *Nature Rev. Mol. Cell Biol.* **8**, 185–194 (2007).

Supplementary Information is linked to the online version of the paper at www.nature.com/nature.

Acknowledgements We would like to thank F. Preitner and B. Thorens for the hyperinsulinaemic euglycaemic clamp studies. M.T. was supported by a fellowship from the Juvenile Diabetes Research Foundation International. The work was supported in part by the Swiss National Science Foundation (SNF, LiverX), the European Community (SIROCCO, ERC and MetaboliMirs) and the Leducq Foundation.

Author Contributions M.T. and M.S. designed the experiments. M.T. performed the experiments and conducted the data analysis. J.H. and M.Z. performed the bioinformatic analysis. M.H.H. provided liver samples and participated in analysis of clinical data. B.B. synthesized antagomirs. A.A. provided liposomal formulations. M.T. and M.S. wrote the paper with input from all co-authors.

Author Information Reprints and permissions information is available at www.nature.com/reprints. The authors declare no competing financial interests. Readers are welcome to comment on the online version of this article at www.nature.com/nature. Correspondence and requests for materials should be addressed to M.S. (stoffel@imsb.biol.ethz.ch).

METHODS

Animals. All mice were males and were maintained on a C57BL/6J background, on a 12-h light/dark cycle in a pathogen-free animal facility. Antagomirs at doses of 15 mg kg^{-1} in 0.2 ml total volume with PBS per injection were administered on two consecutive days through the tail vein of wild-type or *ob/ob* mice at between 6 and 8 weeks of age, or to 12-week-old DIO mice fed on a diet containing 60% fat (Pvolimi Kliba AG) for 8 weeks. Mice were injected with adenoviruses through the tail vein at 1×10^9 plaque-forming units in 0.2 ml PBS. Injection of ad-107/GFP and antagomirs did not effect food consumption compared to that of control-treated animals. Mice were killed 10 d after the adenovirus injection. All animal studies were approved by the Kantonale Veterinärämte Zürich.

BL/Adenovirus injection of fat. Ad-GFP or ad-107/GFP were injected into the perigonal fat at a concentration of 1×10^9 plaque-forming units in 40 μl PBS after surgical exposure. Animals were studied 8 d after injection.

Liver biopsies. Liver biopsy specimens from Caucasian patients were obtained during routine diagnostic work-up at the University Hospital, Basel. Blood samples were collected in the fasting state on the day of the liver biopsy for glucose and plasma-insulin measurements. Most study subjects did not take any medications. A specimen was frozen for research purposes if more than sufficient material was obtained for histopathological examination and if the patient gave his/her written informed consent in accordance with the Ethics Committee of Basel.

Antagomirs. The single-stranded RNAs and modified RNA analogues used in this study consisted of 21–23 nucleotides with modifications as specified: antagomir-103, 5'-u₄c₄uagcccguaacgcu₄g₄c₄u₄-Chol-3'; antagomir-107, 5'-u₄g₄uagcccguaacgcu₄g₄c₄u₄-Chol-3'; MM-antagomir-103, 5'-u₄g₄acagccuagcgcg₄g₄c₄u₄-Chol-3'; antagomir-124 (scrambled), 5'-g₄g₄c₄uagcccguaacgcu₄g₄c₄u₄-Chol-3'. The lower-case letters represent 2'-OMe-modified nucleotides; subscript 's' represents a phosphorothioate linkage; 'Chol' represents cholesterol linked through a hydroxyprolinol linkage¹².

Lipid nanoparticle formulations. Liver-targeting lipid nanoparticle formulations of antagomirs were prepared using the novel ionizable lipid DLin-KC2-DMA (ref. 22). Lipid nanoparticles were composed of DLin-KC2-DMA, distearoyl phosphatidylcholine, cholesterol and mPEG2000-DMG, used at the molar ratio 50:10:38.5:1.5. Antagomirs were formulated in lipid nanoparticles at a total lipid-to-antagomir weight ratio of approximately 11:1.

Generation of recombinant adenovirus. Ad-107/GFP was generated by inserting the PCR-amplified miRNA precursor sequence generated with primers 5'-AATACCCGCATGGAAGCAGGCTAA-3' and 5'-AACATGTCTCAAGGA GAGGACGGT-3' into a GFP-expressing shuttle vector, Ad5CMV K-NpA. Ad-GFP (ViraQuest), which does not contain a transgene, was used as a control.

RNA isolation and northern blotting analysis. 5–30 μg total RNA, isolated using Trizol reagent (Invitrogen), was separated at 15 W on 14% polyacrylamide gels containing formamide, as described in ref. 8.

Real-time PCR. Steady-state mRNA expression was measured by quantitative real-time PCR using the LightCycler 480 SYBR Green Master I Mix (Roche) with a Mx3005P Real-Time PCR System (Stratagene). Transcript levels were normalized to glyceraldehyde 3-phosphate dehydrogenase (GAPDH) or *36B4*, the gene encoding acidic ribosomal phosphoprotein P0 (RPLP0). Primer sequences for real-time PCRs are available on request. MiRNA levels were measured using TaqMan microRNA Assays (Applied Biosystems) and were normalized to U6 levels.

MicroRNA microarray. We used three diabetic groups (*ob/ob* or DIO) and three control groups of mice for each diabetic model. Prior to killing, elevated blood-glucose and insulin levels were confirmed in the diabetic mice. Total RNA, isolated and pooled from the livers of ten mice per group, was labelled using the miRCURY LNA microRNA Power Labelling Kit (Exiqon) and hybridized on miRNA arrays (miRXplore) that carry 1,194 DNA oligonucleotides with the reverse-complementary sequence of the mature RNAs. These arrays cover 728 human, 584 mouse, 426 rat and 122 viral miRNAs, each spotted on the arrays in quadruplicate. The Cy5-labelled miRNAs were normalized to a reference pool of miRNAs that were simultaneously labelled with Cy3. All the data are represented as ratios of logarithmic values between the diabetic and healthy animals \pm s.d.

Assay of luciferase activity and cell culture transfection. 3' UTR sequences were PCR-amplified with specific primers, followed by attB adaptor PCR. Sequences

were cloned into the pDONR221 entry vector using BP Clonase (Invitrogen) and then cloned behind the stop codon of firefly luciferase in the dual renilla/firefly luciferase pEM393 destination vector (gift from E. Miska). HEK 293 cells cultured in 24-well plates were transfected in quadruplicate using Lipofectamine 2000 (Invitrogen) with 100 ng of the final construct per well, together with PBS or 50 nmol of either control or si-103 double-stranded siRNA (Sigma). Cells were collected 42–48 h after transfection and assayed using the Dual-Luciferase Reporter Assay System (Promega). Results were normalized to the renilla luciferase control and expressed relative to the average value of the control, which was treated with PBS. HEK 293 cells were transfected with antagomirs at a concentration of $5.5 \mu\text{g ml}^{-1}$ of medium.

Computer tomography. Animals were scanned using an animal CT-Scanner (LaTheta) at 1 mm intervals from the head to the base of the tail. Images were analysed using the LaTheta Software.

Isolation of stromal-vascular fraction and primary adipocytes. Primary adipocytes and the stromal-vascular fraction from subcutaneous and visceral fat were prepared as previously described^{23,24}. Adipocyte differentiation was induced with insulin, dexamethasone, isobutylmethylxanthine and rosiglitazone when stromal-vascular cells were 80% confluent²⁴. Cells were treated with antagomirs at a concentration of $5.5 \mu\text{g ml}^{-1}$ during the induction period on days 2 and 3.

Automated analysis of adipocyte differentiation. Differentiated cells were fixed with 5% formaldehyde before staining with boron-dipyrromethene (BODIPY) for lipid droplets, Hoechst for nuclei and Syto60 for cytosolic staining (Invitrogen). A total of 25 pictures per well were taken with an automated microscope imaging system (CellWorx). Pictures were analysed using Cell Profiler Software.

Glucose uptake. [¹⁴C]-Spiked glucose uptake, with or without 20 nM insulin stimulation, was measured as previously described²⁴.

Hyperinsulinaemic-euglycaemic clamp studies. Clamps were performed on 8-week-old *ob/ob* mice weighing 40 g. An indwelling catheter for infusion of insulin and glucose was placed into the left femoral vein under isoflurane anaesthesia. Mice were allowed to recover for 6–8 d, until they had regained 95–100% of their initial body weight. After a 5 h fast, a 180 min hyperinsulinaemic-euglycaemic clamp study was conducted in awake, freely moving mice, as previously described^{25,26}.

Adipocyte size. Haematoxylin and eosin staining of 10 μm slices of adipose tissue fixed in 5% paraformaldehyde was performed according to standard procedures²⁷ and images were analysed using Cell Profiler Software. At least 2,000 adipocytes were measured per animal to determine adipocyte size.

Glucose-, insulin- and pyruvate-tolerance tests. Glucose-, insulin- and pyruvate-tolerance tests were performed by intraperitoneal injection of glucose (2 g kg^{-1}), insulin ($0.75 \text{ units kg}^{-1}$, 1 unit kg^{-1} or 2 units kg^{-1} , as indicated in the figures) or pyruvate (2 g kg^{-1}) after an overnight fast for glucose and pyruvate or a 6 h fast for insulin. Blood glucose levels were measured before injection (time 0) and at 15, 30, 60 and 120 min after injection.

Antibodies. The antibodies used were mouse monoclonal anti- γ -tubulin (Sigma-Aldrich), rabbit polyclonals anti-IR β (C-19):sc-711; anti-pIR β (Tyr1162/1163):sc25103, anti-caveolin-1 (N20):sc-894 (Santa Cruz Biotechnology), anti-pAKT and anti-AKT (Cell Signaling).

Statistical analysis. All bars show mean \pm s.d. Significance was calculated using student's *t*-test (*, $P < 0.05$; **, $P < 0.01$; ***, $P < 0.001$).

23. Semple, S. C. *et al.* Rational design of cationic lipids for siRNA delivery. *Nature Biotechnol.* **28**, 172–176 (2010).
24. Hansen, L. H., Madsen, B., Teisner, B., Nielsen, J. H. & Billestrup, N. Characterization of the inhibitory effect of growth hormone on primary preadipocyte differentiation. *Mol. Endocrinol.* **12**, 1140–1149 (1998).
25. Tozzo, E., Shepherd, P. R., Gnudi, L. & Kahn, B. B. Transgenic GLUT-4 overexpression in fat enhances glucose metabolism: preferential effect on fatty acid synthesis. *Am. J. Physiol.* **268**, E956–E964 (1995).
26. Minehira, K. *et al.* Blocking VLDL secretion causes hepatic steatosis but does not affect peripheral lipid stores or insulin sensitivity in mice. *J. Lipid Res.* **49**, 2038–2044 (2008).
27. Preitner, F., Mody, N., Graham, T. E., Peroni, O. D. & Kahn, B. B. Long-term Fenretinide treatment prevents high-fat diet-induced obesity, insulin resistance, and hepatic steatosis. *Am. J. Physiol. Endocrinol. Metab.* **297**, E1420–E1429 (2009).